Kapitza conduction by thin lossy surface layers

1993 J. Phys.: Condens. Matter 5 2063

(http://iopscience.iop.org/0953-8984/5/14/006)

J. Phys.: Condens. Matter 5 (1993) 2063–2080. Printed in the UK

Kapitza conduction by thin lossy surface layers

H Kinder† and K Weiss‡

† Fakultät für Physik E10, Technische Universität München, D-8046 Garching, Federal Republic of Germany

‡ Institut de Microtechnique, Université de Neuchâtel, CH-2000 Neuchâtel, Switzerland

Received 2 November 1992, in final form 18 January 1993

Abstract. We consider the Kapitza conductance due to absorption and emission of phonons by a lossy surface layer which has complex elastic constants and/or complex mass density. We find a series connection of two heat resistances, one between the layer and the solid, and another one between the layer and the helium. A propagator matrix formalism is used to calculate the phonon absorption coefficients, and hence the Kapitza conductance, as a function of angle, frequency and layer thickness in the limit of continuum acoustics with anisotropy. The resulting conductance is large enough to account for the Kapitza anomaly. Most experimental details can be explained if the heat resistance on the solid side is assumed to dominate over that on the helium side. Theoretically we find that both are of the same order at least.

1. Introduction

The Kapitza resistance for heat transport between liquid helium and solids has been a topic of discussion for more than fifty years [1]. The transport by acoustic phonon transmission proposed by Khalatnikov [2] fails to explain the observed large thermal conductance [3] and the strong transmission of phonon pulses [4, 5]. This fact is commonly referred to as the Kapitza anomaly. Haug and Weiss [6] and, independently, Peterson and Anderson [7] (HWPA) suggested that the Kapitza anomaly may be accounted for by complex elastic constants of the solid, which provided a phenomenological model for scattering or absorption of phonons. As a consequence of this, the total reflection of the helium phonons at angles outside the critical cone is no longer complete because the evanescent waves in the solid are attenuated. Although this effect seems to be small it leads to a very effective additional channel of heat transfer because of the large density of states in helium.

This model was qualitatively confirmed by angular distribution measurements in helium by Sherlock and co-workers [8] who observed the critical cone near normal incidence and an additional background at larger angles which carried most of the heat flow. But there were still two major objections to the HWPA model: (i) The imaginary parts required to produce a sufficiently large Kapitza anomaly were comparable to the real parts of the elastic constants. This appeared to be unphysically large in view of ballistic phonon propagation observed in the pulse experiments. (ii) The amplitudes of the evanescent waves depend on the impedance mismatch. Therefore the resulting Kapitza conductance should depend on the helium pressure, on solidification [9, 10], on the replacement of the helium by H, D [11], or even Ar [10], and on the phonon frequency [5]. None of these effects could be found experimentally.

0953-8984/93/142063+18$07.50

New experiments have since shown that the Kapitza anomaly is absent at clean surfaces prepared *in situ* either by cleaving [12, 13] or by laser annealing [14]. This means that the anomaly is caused by surface imperfections, presumably adsorbed water and residual gases. In further experiments the clean surfaces were re-contaminated in a controlled manner by gold atoms [15], and it turned out that less than a monolayer was sufficient to restore the Kapitza anomaly. Similar results were obtained with a coverage of water molecules [16].

These coverages were observed to cause a change from specular reflection to more diffuse scattering at the surface without adjacent helium. With helium, the diffuse part was transmitted while the specular part remained unaffected. The same observation had been made on 'real' surfaces by many authors [17, 13]. So the Kapitza anomaly is clearly related to surface scattering or absorption, and the scattered or re-emitted phonons seem to go preferentially into the helium.

The HWPA model can be adapted to these observations by modelling the adsorbate as a thin layer of an effective lossy medium on the surface. Although this is a crude simplification it should be not too far from reality as long as the mean distance between adatoms is less than a phonon wavelength. For such a disordered layer it seems no longer unphysical to assume a rather high absorption or scattering strength, so that real and imaginary parts of the elastic constants may indeed be of the same order. Moreover, only a thin layer is required for the Kapitza anomaly to occur because of the short penetration depth of the evanescent waves in the solid. Even if the layer is thinner than the penetration depth, we still find appreciable absorption, see section 9. So difficulty (i) can be removed.

As an alternative model, Kinder [18] had made the specific assumption of two-level systems (TLS) on the surface, similar to those observed in glasses [19]. These TLS were assumed to interact with the helium, not via evanescent waves, but directly by the deformation potential. The heat exchange due to absorption and re-emission of phonons of the solid and of the helium by the TLS was strong enough to agree with experiments. The same absorption and re-emission could also be responsible for the apparent surface scattering.

A key argument was that even a small deformation potential allows a very fast relaxation into the helium because of the large density of states. If this relaxation is faster than that into the solid, the diffusely re-emitted phonons will be 'sucked' into the adjacent helium, as observed in the pulse experiments. Also, there will be a bottleneck between the TLS and the solid which dominates the heat transfer. This provides a natural explanation for difficulty (ii), the observed independence of the Kapitza resistance from all helium properties.

Later we have pointed out that the TLS could be described by a lossy surface layer in the same way as discussed above [20], if the expression of Jäckle *et al* [21] was used for the imaginary parts of the elastic constants. In fact, the only remaining difference from a layer–HWPA model was the direct interaction with the helium. So the HWPA model must yield a similar bottleneck to the TLS model if the indirect interaction via evanescent waves is strong enough.

In the present paper we wish to show that this expected bottleneck is a general consequence of backscattering which had been neglected by HWPA [6]. If we take backscattering into account we find essentialy two Kapitza resistances in series, an outer resistance between the helium and the layer, and an inner resistance between the layer and the bulk solid.

The properties of both resistances can be found by calculating the absorption

coefficients as functions of angle, polarization, frequency, and layer thickness. For this purpose we have used a propagator matrix formalism treating the two acoustic half spaces with the lossy intermediate layer exactly. We present numerical results not only for the case of complex elastic constants corresponding to defects with deformation potential coupling, but also for the case of complex mass density corresponding to mass defect scattering.

We find that the inner resistance between the layer and the solid has properties which agree well with the existing experiments. So this indeed seems to be the bottleneck. On the other hand we also get the same magnitude for the outer resistance. So backscattering should clearly not be neglected, but the evanescent wave absorption may not be the only interaction mechanism with the helium.

2. Angular distribution of scattered or re-emitted phonons

The complex elastic constants are a macroscopic model for various microscopic processes which derive energy from an incident wave by scattering or absorption. This energy is scattered or re-emitted into other modes whose frequencies may be the same (scattering) or may have changed (absorption/re-emission). In our present context these modes are the phonons of the bulk solid on one hand, and, via evanescent waves, the phonons of the helium on the other hand. The rotons will be neglected for simplicity. The energy derived from an incident helium phonon does not necessarily contribute to the heat transfer because it has a finite probability of being scattered back into another helium phonon. Similarly, phonons absorbed from the solid side can be backscattered into the solid. To evaluate the backscattering process quantitatively we need not only the absorption but also the emission probabilities for all modes of the helium and the solid.

The scattered or absorbed flux varies across the thickness of the layer, particularly in the case of evanescent waves. Therefore, in principle, the contribution to the backscattered flux should be calculated for each volume element separately and then summed over these elements. In practice, only the average of all modes of the solid and the helium together is relevant to the problem, as will be derived in the next section. This average varies only weakly, however, as long as the bottleneck on the solid side is not extreme. Thus, the numerical results are not significantly altered, and we have treated here the absorption of the layer as a whole for simplicity.

Our macroscopic approach allows us to calculate only the energy flux absorption of the layer for all phonon modes of the solid and the helium. The emitted flux distribution can be obtained in the following way.

The use of macroscopic complex elastic constants and mass density is only meaningful if the response of the medium is sufficiently local. This implies that the underlying microstructure causing the scattering or absorption has a characteristic length scale which is shorter than the phonon wavelength. Likewise the Fourier transform of the microstructure has a distribution which is broader than the length of the phonon wave vector. This means that momentum selection rules are not obeyed during the scattering or absorption processes. There remain only weak polarization selection rules which can be neglected in the present context as we do not expect any observable consequences. So the pattern re-emitted at a given frequency has always the same angle and polarization dependence, regardless of which phonon had been absorbed. Thus, the total flux pattern at this frequency, re-emitted from all

absorbed phonons in thermal equilibrium, is also the same. But this total pattern is, by detailed balance, the same as the absorption pattern. So the flux re-emitted at a given frequency has always the same dependence on angle and polarization as the flux absorption at the same frequency.

Before we actually calculate the flux absorption we wish to discuss the consequences of the phonon backscattering for the Kapitza conduction.

3. Kapitza conduction including backscattering

The energy flux absorbed from a single incident phonon with wave vector k is given by

$$q_k^i = (\hbar\omega_k/\Omega_i)v_{g\perp k}^i A_k^i \tag{1}$$

where the index i stands for either helium (h) or solid (s), Ω_i is the normalization volume, $v_{g\perp k}^i$ is the normal component of the group velocity, A_k^i is the flux absorption coefficient of the layer, and k is meant to include both wave vector and polarization index.

In general, the flux absorbed at frequency ω is re-emitted in a distribution $f(\omega, \omega')$ of frequencies ω'. Conservation of flux requires

$$\int d\omega' f(\omega,\omega') = 1. \tag{2}$$

As discussed in the previous section, the angular and polarization distribution of the phonons re-emitted at ω' is the same as that of the flux absorption at ω'. So the normalized angular and polarization distribution re-emitted into medium j at frequency ω' is given by $q_{k'}^j/[W_h(\omega')+W_s(\omega')]$, where we have used the abbreviation

$$W_i(\omega') = \sum_{\omega_{k''}=\omega'} q_{k''}^i. \tag{3}$$

The symbol $\sum_{\omega_k=\omega'}$ denotes the summation over the surface of constant frequency ω', so that $\int d\omega' \sum_{\omega_k=\omega'} \equiv \sum_k$. For the evaluation see sections 7 and 8.

Thus, the flux pattern re-emitted into medium j due to a single phonon of frequency ω incident from medium i is

$$V_{kk'}^{ij} = q_k^i f(\omega_k, \omega_{k'}) q_{k'}^j/[W_h(\omega_{k'}) + W_s(\omega_{k'})]. \tag{4}$$

In the Kapitza problem the incident phonons have Bose–Einstein distributions, $n(\omega, T_i)$, and the net heat current due to all phonons absorbed from the helium and re-emitted into the solid, and vice versa, is obtained by summation of (4):

$$Q = \int d\omega d\omega' f(\omega, \omega') \frac{n(\omega, T_h)W_h(\omega)W_s(\omega') - n(\omega, T_s)W_s(\omega)W_h(\omega')}{W_h(\omega') + W_s(\omega')}. \tag{5}$$

While the $W_i(\omega)$ will be calculated later in this paper, the distribution function $f(\omega, \omega')$ is not known in general. But we can discuss two limiting cases, elastic scattering on one hand, and full inelastic thermalization on the other.

In the first case of elastic scattering we have simply $f(\omega, \omega') = \delta(\omega, \omega')$, so that, for $|T_h - T_s| \ll T$,

$$\dot{Q} = \int d\omega \frac{W_h(\omega) W_s(\omega)}{W_h(\omega) + W_s(\omega)} \frac{\partial n(\omega, T)}{\partial T} (T_h - T_s). \tag{6}$$

For simplicity we have assumed that the absorption coefficients A^i_k are independent of temperature. The generalization is obvious. We see that the heat flux is essentially determined by two Kapitza resistances in series, one for the helium side and one for the solid side.

In the second case the re-emitted spectrum is assumed to be fully thermalized to an intermediate temperature T_r. The flux re-emitted into each outgoing phonon mode is then

$$n(\omega', T_r) q^j_{k'} \tag{7}$$

and the re-emitted phonons have no memory of the incident frequencies, i.e. the distribution function $f(\omega, \omega') \equiv f(\omega')$ does not depend on ω. By summing (4) over all incident phonons of both half spaces and comparing the result with (7) we find

$$f(\omega') = n(\omega', T_r)[W_h(\omega') + W_s(\omega')] \Big/ \int d\omega [n(\omega, T_h) W_h(\omega) + n(\omega, T_s) W_s(\omega)]. \tag{8}$$

In steady state, T_r adjusts itself so that the flux is conserved, that is, equation (2) holds. So we obtain an implicit equation defining T_r by integration of (8) with respect to ω'. For $|T_h - T_s| \ll T$ this equation can be easily solved:

$$T_r = \frac{T_h \int d\omega\, W_h(\omega) \partial n(\omega, T)/\partial T + T_s \int d\omega\, W_s(\omega) \partial n(\omega, T)/\partial T}{\int d\omega\, (W_h(\omega) + W_s(\omega)) \partial n(\omega, T)/\partial T}. \tag{9}$$

Using (9), (8) and (5), we get for the net heat current in the case of full thermalization after some algebra

$$\dot{Q} = \frac{\left[\int d\omega\, W_h(\omega) \partial n(\omega, T)/\partial T\right] \left[\int d\omega\, W_s(\omega) \partial n(\omega, T)/\partial T\right]}{\left[\int d\omega\, W_h(\omega) \partial n(\omega, T)/\partial T\right] + \left[\int d\omega\, W_s(\omega) \partial n(\omega, T)/\partial T\right]} (T_h - T_s). \tag{10}$$

Here we have a true series connection of an inner and an outer Kapitza resistance, while in the case of elastic scattering, equation (6), the series connection is made for each frequency separately.

If one of the resistances is much larger than the other, it will dominate the overall Kapitza resistance. Therefore, the inclusion of backscattering leads to the remarkable fact that any changes on the helium side have no influence if the resistance of the solid side dominates. To examine whether this is really the case for our present model of coupling by evanescent waves we must explicitly calculate the absorption coefficients. We used a concise method to solve the acoustics problem which will be presented in the next section before discussing the various numerical results.

4. Acoustics in layered anisotropic media

Anisotropy of crystals and focusing effects play an important role in all phonon propagation experiments. Therefore we wish to calculate the absorption coefficients of the dissipative layer for anisotropic media of arbitrary surface orientation. For this purpose we use the propagator matrix approach which has been developed in seismology [22]. Because we are applying it here to a phonon problem for the first time, we shall give a brief outline.

We start with the Fourier transform of the homogeneous equation of motion for each medium, the solid, the layer, and the helium:

$$-\rho\omega^2 u_i = \mathrm{i}k_j \tau_{ij} \qquad i, j = 1,2,3 \tag{11}$$

where ρ is the mass density which may be complex, u_i is the displacement vector, k_j is the wave vector, and τ_{ij} is the stress tensor. The index for the different media is omitted here. We adopt the convention of summing over repeated indices. Hooke's law for each medium is

$$\tau_{ij} = \mathrm{i}c_{ijkl}k_k u_l \tag{12}$$

with the elastic constants c_{ijkl} which may in general be complex as well. The parallel component of the wave vector is conserved at the plane boundaries of the layer. Therefore the wave fields in each of the three media will be linear combinations of solutions with the same $k_\parallel$. This $k_\parallel$ must always be real everywhere, because it is real for the incident wave. Traditionally, one finds solutions of (11) and (12) for a given $k_\parallel$ by eliminating all components of τ_{ij}. This yields the Christoffel equation whose determinant is a sixth-degree polynomial in $k_\perp$, the normal component of the wave vector. In principle, the zeros of the polynomial can be found. In practice, the coefficients of the polynomial fill pages with complicated expressions which are not well suited for numerical calculations [23]. It is much more convenient to transform the task into an eigenvalue problem.

This can be achieved by eliminating only the components of τ_{ij} with $i, j = 1, 2$ while keeping the normal stresses τ_{i3}, $i = 1,2,3$, as independent variables. Thereby we have chosen the x_3 axis as the surface normal. This implies $k_{\parallel 3} = 0$ and $k_{\perp 1} = k_{\perp 2} = 0$. Then one obtains from (11) and (12)

$$-\rho\omega^2 u_i = -\mathrm{i}k_{\parallel j} c_{ijkl}(k_{\parallel k} + k_{\perp k})u_l + \mathrm{i}k_{\perp 3}\tau_{i3}. \tag{13}$$

In addition, there remains for the third component of (12)

$$\tau_{i3} = \mathrm{i}c_{i3kl}(k_{\parallel k} + k_{\perp k})u_l. \tag{14}$$

Together, (13) and (14) form a set of six homogeneous linear equations for the six variables u_i and τ_{i3}. We introduce the motion-stress vector [22]

$$(f_i) = \begin{bmatrix} -\mathrm{i}\omega u_1 \\ -\mathrm{i}\omega u_2 \\ -\mathrm{i}\omega u_3 \\ \tau_{13} \\ \tau_{23} \\ \tau_{33} \end{bmatrix} \equiv \begin{bmatrix} -\mathrm{i}\omega u_i \\ \tau_{i-3,3} \end{bmatrix} \qquad \begin{matrix} i = 1,2,3 \\ i = 4,5,6 \end{matrix} \tag{15}$$

and collect all factors of $k_\perp$ on the right-hand side. Then (13) and (14) take on the form

$$A_{ij} f_j = B_{ij} f_j s_\perp \qquad i, j = 1, \ldots, 6 \tag{16}$$

where we have introduced the slowness $s = q/\omega$. The coefficients are given by

$$(A_{ij}) = \begin{matrix} j = 1,2,3 \\ \\ \end{matrix} \quad \begin{matrix} j = 4,5,6 \\ \\ \end{matrix}$$

$$\begin{bmatrix} -\rho\delta_{ij} + c_{iklj} s_{\parallel k} s_{\parallel l} & 0 \\ c_{i-3,3kj} s_{\parallel k} & \delta_{ij} \end{bmatrix} \quad \begin{matrix} i = 1,2,3 \\ i = 4,5,6 \end{matrix} \tag{17}$$

$$(B_{ij}) = \begin{matrix} j = 1,2,3 \\ \\ \end{matrix} \quad \begin{matrix} j = 4,5,6 \\ \\ \end{matrix}$$

$$\begin{bmatrix} -c_{ik3j} s_{\parallel k} & \delta_{i,j-3} \\ -c_{i-3,33j} & 0 \end{bmatrix} \quad \begin{matrix} i = 1,2,3 \\ i = 4,5,6. \end{matrix} \tag{18}$$

Here we have applied the notation introduced in (15) for columns and rows. Equation (16) is a generalized eigenvalue problem which we solve directly by a library routine (IMSL). This has numerical advantages over solving the normal form

$$(B^{-1})_{ij} A_{jk} f_k = f_k s_\perp. \tag{19}$$

The six eigenvalues $s_{\perp\alpha}$ are the intersections of the line of constant $s_\parallel$ with the slowness surface, as indicated in the inset of figure 1(*a*).

Some of the $s_{\perp\alpha}$ may be complex conjugate at larger $s_\parallel$, leading to inhomogeneous, evanescent waves. With losses, all $s_{\perp\alpha}$ have finite imaginary parts. The eigenvectors corresponding to each $s_{\perp\alpha}$ contain the particle velocities and normal strains of this mode. Remarkably these are the quantities conserved in the boundary problem which we shall discuss in the next section. It will be convenient to arrange all six eigenvectors as the columns of a matrix $E_{i\alpha}$ and to normalize each column so that

$$E_{1\alpha}^2 + E_{2\alpha}^2 + E_{3\alpha}^2 = 1. \tag{20}$$

For the special case of an isotropic medium, $E_{i\alpha}$ can be written down explicitly. We restrict ourselves here to the case of $c_{44} = 0$, appropriate for liquid helium:

$$E_{i\alpha}^{\mathrm{h}} = v \begin{matrix} \alpha = 1, \ldots, 6 \\ \\ \\ \\ \\ \\ \end{matrix} \quad \begin{bmatrix} s_{\parallel 1} & s & 0 & s_{\parallel 1} & s & 0 \\ s_{\parallel 2} & 0 & s & s_{\parallel 2} & 0 & s \\ s_{\perp 3} & 0 & 0 & -s_{\perp 3} & 0 & 0 \\ 0 & 0 & 0 & 0 & 0 & 0 \\ 0 & 0 & 0 & 0 & 0 & 0 \\ -\rho & 0 & 0 & -\rho & 0 & 0 \end{bmatrix} \quad i = 1, \ldots, 6. \tag{21}$$

Here, $v = 1/s = \sqrt{c_{11}/\rho}$ is the phase velocity in the liquid, and $s_{\perp 3} = \sqrt{s^2 - (s_{\parallel 1}^2 + s_{\parallel 2}^2)}$. The columns with $\alpha = 1$ and $\alpha = 4$ are the incoming and outgoing longitudinal waves while columns 2, 3, 5 and 6 represent the degenerate transverse waves. Equation (21) defines the boundary problem of the liquid completely, including the so-called Khalatnikov boundary conditions.

5. Calculation of the absorption and transmission coefficients

Now that the eigenvalue problem is solved for given $s_{\parallel}$, we obtain the general wave field in each medium as a linear combination of the corresponding eigenmodes

$$f_i(z) = E_{i\alpha} \exp(\mathrm{i}\omega s_{\perp\alpha} z) w_\alpha \equiv E_{i\alpha} \Lambda_{\alpha\beta}(z) w_\beta \tag{22}$$

where w_β are the amplitudes of the eigenmodes in the linear combination and $\Lambda_{\alpha\beta}(z) \equiv \delta_{\alpha\beta} \exp(\mathrm{i}\omega s_{\perp\alpha} z)$ is the so-called phase matrix [22].

The motion-stress vector f must be continuous across the boundaries. We introduce the indices s, l, and h for the solid, the layer, and the helium, respectively, and we denote the boundaries by $z = z_s$ and $z = z_h$, so that the layer thickness is $d = z_s - z_h$. Then we can write down the boundary conditions

$$E^s_{i\alpha} \Lambda^s_{\alpha\beta}(z_s) w^s_\beta = E^l_{i\alpha} \Lambda^l_{\alpha\beta}(z_s) w^l_\beta \tag{23a}$$

$$E^l_{i\alpha} \Lambda^l_{\alpha\beta}(z_h) w^l_\beta = E^h_{i\alpha} \Lambda^h_{\alpha\beta}(z_h) w^h_\beta. \tag{23b}$$

Eliminating the amplitudes of the layer, w^l_β, from (23*a*) and (23*b*) yields

$$E^s_{i\alpha} \Lambda^s_{\alpha\beta}(z_s) w^s_\beta = P^l_{ij}(z_s - z_h) E^h_{j\alpha} \Lambda^h_{\alpha\beta}(z_h) w^h_\beta \tag{24}$$

where we have used the propagator matrix of the layer defined by

$$P^l_{ij}(z_s - z_h) = E^l_{i\alpha} \Lambda^l_{\alpha\beta}(z_s) \Lambda^{-1}_{\beta\gamma}(z_h) E^{-1}_{\gamma j} = E^l_{i\alpha} \exp(\mathrm{i}\omega s_{\perp\alpha} d) E^{-1}_{\alpha j}. \tag{25}$$

The same procedure can also be applied to multiple layers by multiplying the corresponding propagator matrices. We have made use of this possibility here to study the influence of an additional layer of solid helium, as will be briefly discussed in section 9.

Equation (24) is a linear system which couples the amplitudes of the modes in both half spaces. They must be sorted for incident and outgoing directions in order to obtain transmission and reflection coefficients.

Sorting of propagating bulk modes with real $s_\perp$ is done with respect to the sign of $v_{g\perp}$. The simplest way to obtain this quantity in the present context is via the normalized energy flux of the mode:

$$v_{g\perp\alpha} = (1/\rho_\alpha) \operatorname{Re}\{E^*_{i\alpha} E_{i+3,\alpha}\} \tag{26}$$

where the summation index i runs from 1 to 3, and the $E_{i\alpha}$ are normalized according to (20). ρ_α denotes the density of the medium to which the mode belongs. Sorting of evanescent waves with complex $s_\perp$ is done with respect to the sign of $\operatorname{Im}\{s_{\perp\alpha}\}$.

Equation (24) can now be rearranged so that the terms with incident and outgoing modes are placed on the right- or left-hand side, respectively. Further, the phase matrices multiplying w^s_β and w^h_β can be omitted because we are interested only in the absolute values of the transmission and reflection coefficients. These are eventually obtained by setting one of the incident amplitudes to unity while putting all others to zero, and then solving the inhomogeneous linear system for the outgoing amplitudes. We have done this numerically, simultaneously for all incident modes of the solid ($\alpha = 1,2,3$) and the incident longitudinal mode of the helium ($\alpha = 4$).

We denote the resulting amplitude coefficients for transmission or reflection by $a_{\alpha\beta}$ where $\beta = 1,2,3,4$ indicates the outgoing modes. The corresponding energy flux coefficients are then given by

$$K_{\alpha\beta} = (\rho_\beta v_{g\perp\beta}/\rho_\alpha v_{g\perp\alpha})|a_{\alpha\beta}|^2 \tag{27}$$

without summing over α or β. The energy flux is conserved if there is no dissipation, and $\sum_{\beta=1}^{4} K_{\alpha\beta} = 1$ can then serve as a numerical test. With dissipation in the layer, we define the absorption coefficient of the αth incident mode as

$$A_\alpha = 1 - \sum_{\beta=1}^{4} K_{\alpha\beta}. \tag{28}$$

To gain insight into the various phenomena, we will give some numerical examples for the absorption and transmission coefficients in the following sections. First we concentrate on the $s_\parallel$ dependence.

6. Dependence of transmision and absorption coefficients on $s_\parallel$

It is useful to study the behaviour of the transmission and absorption coefficients as a function of the parallel slowness, $s_\parallel$, because it is conserved at the interfaces. This way the effects of mode conversion become more obvious. In all numerical examples we used $\rho = 0.14$ g cm^{-3} and $v = 240$ m s^{-1} for the liquid helium [24]. For the solid we have always chosen silicon with $\rho = 2.331$ g cm^{-3}, $c_{11} = 167.5$ GPa, $c_{12} = 65$ GPa and $c_{44} = 80.1$ GPa [25].

The formalism works equally well for all orientations of the surface by rotating the fourth-rank tensor c_{ijkl}:

$$c_{ijkl} = R_{im} R_{jn} R_{ko} R_{lp} c_{\mu_{mn}\mu_{op}} \tag{29}$$

where the R_{ij} are the direction cosines between the original and the rotated basis, and the $c_{\mu_{mn}\mu_{op}}$ are the elastic constants in Voigt's notation which we translate to tensor indices by the matrix

$$(\mu_{mn}) = \begin{bmatrix} 1 & 6 & 5 \\ 6 & 2 & 4 \\ 5 & 4 & 3 \end{bmatrix}. \tag{30}$$

In the examples of this section we have picked the orientation by the random numbers (83, 64, 25). On this surface we selected for $s_\parallel$ a random angle of $-66°$ with respect to the projection of the (100) axis on the surface.

For the elastic constants of the intermediate layer we have chosen the same absolute values as for silicon, but multiplied them by a phase factor, $\exp i\delta$, with $\tan\delta = 1$. In the case of TLS with a deformation potential of $M = 3$ eV [26] this requires a density of states [21] of $N(E) = c_{44}\tan\delta/2\pi M^2 = 5 \times 10^{33}$ erg^{-1} cm^{-3}. For comparison, a value of 8×10^{32} erg^{-1} cm^{-3} was obtained for vitreous silica from the low-temperature specific heat [27]. In reality, a disordered adsorbate is probably softer than silicon and contains more TLS than bulk vitreous silica.

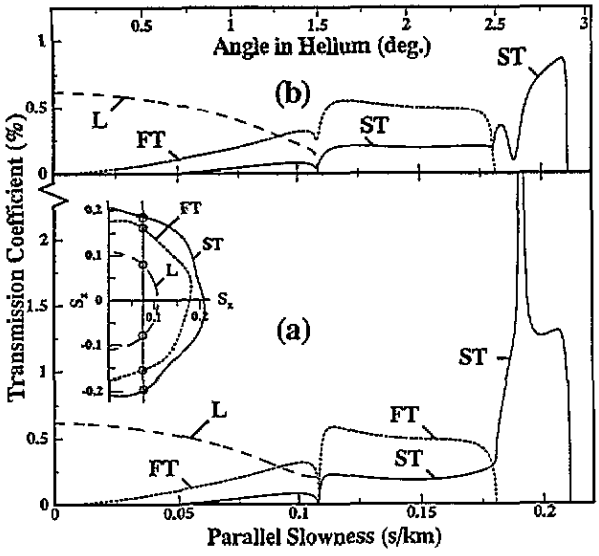

Figure 1. Acoustic transmission coefficient from silicon into helium as a function of the parallel component of the slowness: (*a*) without a lossy layer; (*b*) with a layer of $d\omega = 1$ km s^{-1} ($d = 0.8$ nm at $f = 200$ GHz) and elastic losses ($\tan\delta = 1$). Inset: corresponding cross section of slowness surface.

Figure 1 shows the transmission coefficients according to (27) from the solid into the helium as a function of $s_{\|}$ for longitudinal (L), fast transverse (FT), and slow transverse (ST) phonons. The corresponding angle of propagation in k space can be found in the inset which we have drawn for the same orientation, with $v_{gz} > 0$ for incident waves. The angle in helium is displayed in figure 1(*b*).

In figure 1(*a*), the thickness of the layer was actually chosen to be zero. This means that the absorbing layer is absent, and we deal with Khalatnikov's direct acoustic transmission only. This is interesting in itself because we are studying here the anisotropic generalization for the first time. Both transverse modes are now transmitted, as expected. An interesting feature is the sharp peak at 0.19 s km^{-1}. An analysis of the displacements shows that it is due to a pseudo-surface wave. In the present orientation the peak rises to a maximum of about 40% transmission. In other directions, it can even rise to 100%. While the phenomenon can be observed by ultrasonic techniques [28] it does not contribute appreciably to the Kapitza conduction because the peak is very narrow.

In figure 1(*b*), the thickness of the layer is finite. In fact, the results depend, according to (25), only on the product of thickness times frequency, $d\omega$, as long as the loss angle δ is independent of ω. Here we chose $d\omega = 1$ km s^{-1}. This corresponds, for example at $\omega/2\pi = 200$ GHz, to a thickness of 0.8 nm. A drastic change has occurred at the pseudo-surface wave which is now so strongly damped that it causes a dip rather than a peak in the transmission. All other features of the curves are only slightly modified. Clearly, the layer does not act as a matching device, since the overall transmission remains small.

While the layer has little influence on the direct transmission, it does lead to a strong absorption of phonons. The absorption coefficients according to (28) are plotted in figure 2 for incidence from the solid side. In figure 2(*a*), we used again

$d\omega = 1$ km s^{-1}, and in figure 2(*b*) 2 km s^{-1} (16 Å at 200 GHz). Near normal incidence, i.e. $s_{\parallel} \simeq 0$, the absorption is relatively weak, particularly for the thinner layer of figure 2(*a*). This can be understood as follows.

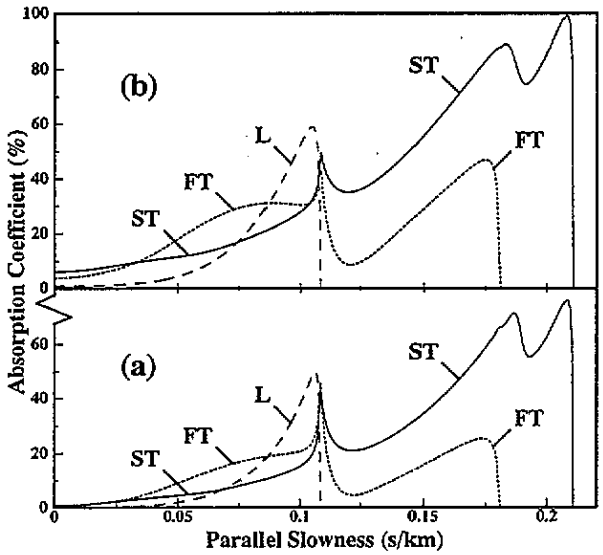

Figure 2. Absorption coefficient of a layer with elastic losses as a function of $s_{\parallel}$ for (*a*) $d\omega = 1$ km s^{-1} and (*b*) $d\omega = 2$ km s^{-1}.

Due to the strong acoustic mismatch to the helium, the surface of the layer is nearly free, so that the stress is vanishing. Consequently, there is also a node of the strain for waves at normal incidence. A sufficiently thin layer on the surface is therefore not exposed to strain and cannot dissipate any energy even though its elastic constants are complex. However, this argument holds only for normal incidence. When the wave fronts are inclined with respect to the surface, the phase varies along the layer, straining it in the lateral direction. This leads to the increasing absorption at increasing $s_{\parallel}$.

Superposed on this general behaviour are peaks at 0.11 s km^{-1} in figure 2 on the curves of both transverse modes. At this point the longitudinal mode has its maximum $s_{\parallel}$, so that its group velocity is parallel to the surface and therefore its interaction with the layer is strong. This leads also to a dissipation of the transverse waves via mode conversion at the surface. The peaks have the same positions and a similar explanation as the halo of 'critical cone channelling' observed by Koos *et al* [29] in a different context.

The thicker layer of figure 2(*b*) already shows effects of finite thickness. At normal incidence there is now significant absorption because the layer feels the increasing strain inside the solid away from the node at the surface. The effect is stronger for the transverse waves because of their shorter wavelengths. On the other hand, the peaks of critical cone channelling are now less significant in comparison with the overall level. They disappear completely at $d\omega \simeq 3$ km s^{-1} when the overall level approaches unity. So the peaks may serve in experiments to estimate the thickness of the lossy layer.

The effects discussed so far are specific for elastic dissipation by complex elastic constants. In the case of a complex mass density, corresponding to dissipation by mass–spring systems, we encounter a different situation. This is shown in figure 3 for the thinner layer with $d\omega = 1$ km s^{-1} (8 Å at 200 GHz), and tan $\delta = 1$. Now the absorption is strong for all angles of incidence, because the complex mass couples to the large particle velocity near the surface. A similar behaviour is also obtained for rough surfaces without an adlayer [30]. So a vanishing absorption near normal incidence may serve in experiments as a specific signature of the elastic dissipation due to deformation potential coupling of defects and, at the same time, as an indication that the surface is smooth on the scale of a wavelength.

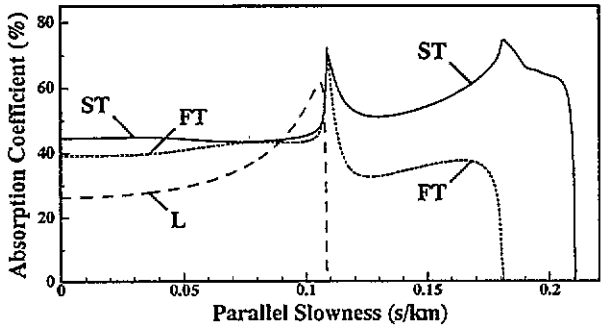

Figure 3. Layer with complex mass density (dynamic losses) at $d\omega = 1$ km s^{-1}.

Phonons incident from the helium side are absorbed in the layer via their evanescent waves. This is shown in figure 4 for (*a*) elastic and (*b*) dynamic dissipation, with $d\omega = 1$ km s^{-1}. The overall absorption is quite small, of the order of 10^{-3} for (*a*) and even weaker for (*b*). This comes from the large impedance mismatch between the helium and the layer. Sharp structures are found at small $s_{\parallel}$ near normal incidence. For a better resolution we have redrawn the curves with the horizontal scale expanded by a factor of 10, and the vertical scale compressed by a factor of 25 (the dotted curves). We find two distinct peaks. The smaller one is due to the pseudo-surface wave seen also in figure 1, and the larger one is caused by the genuine Rayleigh mode which has an $s_{\parallel}$ exceeding that of the bulk modes. Note that the peak positions in traces (*a*) and (*b*) are slightly shifted against one another, due to the different method of attenuation.

For larger $s_{\parallel}$, near 2 s km^{-1} on the normal scale of the traces, there is a hump where position depends on $d\omega$ and on δ. An inspection of the wave field shows that this is a thickness resonance of the oscillatory part of the evanescent wave which arises from the imaginary parts of the elastic constants or the density.

The peak at the largest $s_{\parallel}$, near grazing incidence, appears only in the absorption coefficient. When multiplied by $v_{g\perp}$ to yield the flux according to (1), a constant course results which eventually falls to zero at 90°. This compares well with the experiments by Sherlock *et al* [8] who found a nearly constant flux up to angles of 80° at the lowest heater temperature of 0.9 K.

The $s_{\parallel}$ dependence is not sufficient for analysing experiments with angular resolution in the solid. In this case the Kapitza pattern must be translated into

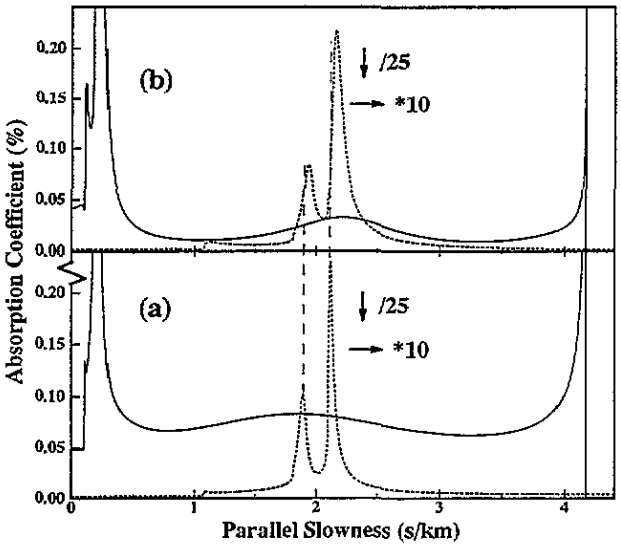

Figure 4. Absorption coefficient of phonons incident from the helium for (*a*) elastic and (*b*) dynamic losses. Dotted curves are rescaled as indicated. The peaks are due to the pseudo-surface wave and the Rayleigh mode.

position space, that is, the phonon focusing effects must be taken into acount. The resulting flux pattern on the solid side will be considered next.

7. Energy flux pattern including focusing in the solid

An incoherent phonon source, like a heat pulse generator, a tunnel junction, or a laser focus, emits phonons into a crystal with v_{gz} pointing away from the source. For a given frequency, the occupation numbers $n(\omega)$ of all k states and polarizations are approximately equal. Then the flux absorbed by a dissipative layer at the far surface of the crystal in a surface element $\Delta x \Delta y$ at a position x, y is

$$I(x, y)\Delta x \Delta y = \sum_{\alpha} \sum_{k \in B(x,y)} n(\omega_k) \frac{\hbar \omega_k}{\Omega} v^{\alpha}_{gzk} A^{\alpha}_k . \tag{31}$$

The k sum is restricted, so that the surface element is hit, to a range $B(x, y)$ defined by the conditions $x \leqslant v_{gx} D/v_{gz} < x + \Delta x$, and $y \leqslant v_{gy} D/v_{gz} < y + \Delta y$ where D is the crystal thickness, and v_{gz} is positive.

For $A_k \equiv 1$, (31) is the correct expression for phonon focusing. In the literature, phonon focusing is usually calculated by a Monte Carlo technique [31] where the phonon directions are chosen at random, and Lambert's cosine law is accounted for by a weight factor proportional to the cosine of the angle of the k vector. We note from (31) that this is incorrect in the anisotropic case. Rather, it is evident from the factor v_{gz} that the cosine of the group velocity angle appears. A second problem of the usual Monte Carlo technique is that the relative weights of the polarizations are not known. So they were approximated by Debye densities of states [32].

All of these difficulties can be avoided if (31) is evaluated properly. For this purpose we replace the k sum by an integral and use the fact that

$$v_{gz}\mathrm{d}k_z = (\partial\omega/\partial k_z)\mathrm{d}k_z = \mathrm{d}\omega. \tag{32}$$

This automatically takes care of the generalized Lambert's law, and we obtain

$$I(x, y)\Delta x\Delta y = \frac{\hbar}{16\pi^3}\int \mathrm{d}\omega n(\omega)\omega^3 \sum_\alpha \int_{B(x,y)} \mathrm{d}^2 s_\parallel A_\alpha(\omega, s_\parallel). \tag{33}$$

The $s_\parallel$ integration is taken over the extremal cross sections of the three polarization sheets of the slowness surface. Their relative sizes determine the relative weights of the polarizations exactly.

We evaluate the $s_\parallel$ integral for given ω by scanning s_x and s_y. This reduces the scatter of the data in comparison with a Monte Carlo technique. Moiré patterns are avoided by adding small random vectors to the selected $s_\parallel$. During the scan, the results are sorted into an x–y histogram defined by the $B(x, y)$.

For monochromatic phonons, the histogram reflects directly the flux pattern absorbed from the solid. More or less the same is expected for heat pulses, because $A_\alpha(\omega, s_\parallel)$ does not depend strongly on ω. So we can predict the outcome of heat pulse transmission experiments complementary to those of Sherlock *et al* [8], with specified propagation direction in the solid, and the full solid angle on the helium side. Some experiments with a fixed normal incidence on the solid side have been reported [33]; the full angular distribution will be published shortly [34].

Figure 5 shows the predicted flux pattern for Si (001) under various conditions. All three polarizations were added together here. The lateral dimensions of the plots are $1.25D$, where D is the crystal thickness, and the grid width is $D/40$. The relative vertical scale factors are 1, 6, 2 and 300 for (*a*), (*b*), (*c*) and (*d*), respectively.

Figure 5(*a*) is the focusing pattern, or alternatively, the black-body case, with $A_\alpha \equiv 1$. This is shown for comparison. In figures 5(*b*) and (*c*) we assumed a layer with complex elastic constants and density, respectively ($d\omega = 1$ km s^{-1}, $\tan\delta = 1$). In both cases the critical cone channelling leads to a ring shaped halo with pronounced maxima mainly on the ST ridges (diagonal lines in figure 5). As mentioned before, this phenomenon disappears for thicker layers, around $d\omega \simeq 3$ km s^{-1}.

Comparison of figure 5(*b*) with figure 5(*c*) shows that the absorption at normal incidence is still reduced, although this effect is less pronounced than in figure 2. So it is still possible to distinguish elastic and dynamic losses experimentally. One should keep in mind, however, that the node of the elastic strain (see section 6) exists only at smooth surfaces. So the effect for elastic losses can be masked by roughness in an experiment.

It is interesting to compare these results with the pattern expected for direct acoustic transmission (see figure 5(*d*)). The most pronounced feature is the complete absence of the FT ridges parallel to the cubic axes in the surface. These have polarizations nearly parallel to the surface and hence do not couple to the helium. Clearly, the angular distribution on the solid side can be used as a 'fingerprint' of the transport mechanism.

While we have concentrated so far on the angular distribution of the absorbed or emitted phonons we wish to discuss briefly also the frequency and thickness dependence.

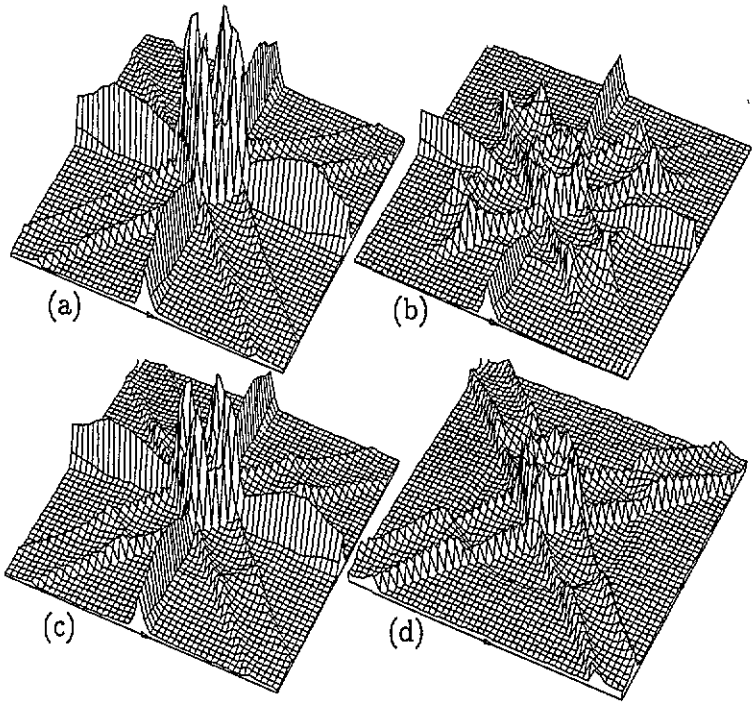

Figure 5. Time-integrated flux patterns on an Si (001) surface due to a point source on the far face of the crystal: (*a*) the focusing pattern alone; (*b*) the flux absorbed in a layer with elastic losses; (*c*) with dynamic losses and (*d*) for direct (Khalatnikov) transmission.

8. Frequency and thickness dependence of the absorption coefficients

The frequency and thickness dependence of the absorption coefficients determines the variation of the Kapitza resistance with temperature. If the bottleneck on the solid side is strong enough, as suggested by the experiments, then both (6) and (10) reduce to the same expression

$$\dot{Q} = \int \mathrm{d}\omega W_s(\omega)(\partial n(\omega, T)/\partial T)(T_h - T_s). \tag{34}$$

Therefore we restrict ourselves here to a discussion of $W_s(\omega)$. According to (3) and following the reasoning of the last section we can write this as

$$W_s(\omega) = \frac{\hbar}{16\pi^3}\omega^3 \sum_\alpha \int \mathrm{d}^2 s_\parallel A_\alpha(\omega, s_\parallel). \tag{35}$$

The $s_\parallel$ integration is done in the same way as before, but without sorting into a histogram. For a better overview we have not plotted $W_s(\omega)$ directly but normalized to the black-body case W_0 with $A_\alpha \equiv 1$. $W_s(\omega)/W_0$ can be viewed as the angular average of the absorption coefficient. This quantity is displayed as a function of $d\omega$ in figure 6. We have again assumed Si (001), and a layer with the same absolute values

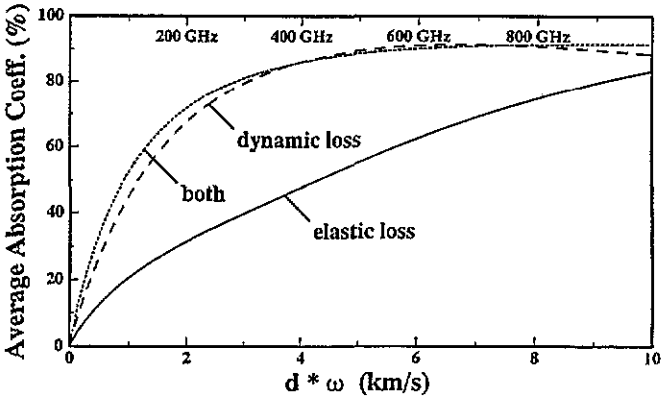

Figure 6. Angular average of absorption coefficient versus $d\omega$ of the layer. The upper frequency scale is valid for a layer thickness $d = 1.6$ nm.

of the material parameters, but with $\tan\delta = 1$ for elastic losses, dynamic losses, or both. For convenience, we have added a scale for the frequency $f = \omega/2\pi$ (upper abscissa) corresponding to a thickness of 1.6 nm.

We see in figure 6 that the absorption coefficient rises nearly linearly with frequency, and then saturates. For the Kapitza conductance this implies a T^4 law at low temperatures, and a T^3 law at higher temperatures, as observed experimentally [3]. So the underlying assumption of a frequency independent loss angle seems to be appropriate. The crossover frequency depends on the layer thickness and the various parameters entering the problem. Here we obtain, e.g. for $d = 1.6$ nm, crossover frequencies of 600 GHz (elastic), 200 GHz (dynamic), and 180 GHz (both), corresponding to temperatures of 7.5 K, 2.5 K, and 2.2 K respectively. The last case is closest to the experimental value of roughly 1 K.

So the properties of W_s alone agree well with experiment, suggesting that $W_h \gg W_s$ is fulfilled experimentally. It remains to investigate whether this is also true theoretically for the mechanism of evanescent wave absorption.

9. Ratio of inner and outer Kapitza resistance

Our model seems to be useful as far as the calculation of the inner Kapitza resistance is concerned. For the outer resistance this is not so clear. In the helium, phonons have much shorter wavelengths, so that the evanescent waves vary rapidly in space as well. So the assumption of locality can be questioned, and also the assumption of a flat surface. Nevertheless it is worthwhile to see how far one can proceed with these simple assumptions.

The ratio between the inner and outer resistances is determined by $W_h(\omega)/W_s(\omega)$. We have calculated this ratio according to (35) for Si (001) at $d\omega = 2$ km s^{-1} for various sets of parameters and display the results in table 1. Besides the loss angles of the elastic constants and density of the layer we have also varied the magnitudes of these material parameters which we scale with respect to the silicon values by a factor F. In some cases we have added a solid helium layer

Table 1. Ratio of inner and outer Kapitza resistance, W_h/W_s, and average flux absorption coefficient for the solid side, W_s/W_0, at $d\omega = 2$ km s^{-1}. Parameters are the loss tangents of elastic constants and mass density ($\tan\delta_c$ and $\tan\delta_\varrho$), a reduction factor for the material parameters with respect to silicon (F), and the presence of a solid helium layer (SHL).

$\tan\delta_c$	$\tan\delta_\varrho$	F	SHL	W_h/W_s	W_s/W_0
1	0	1	no	0.60	0.31
0	1	1	no	0.091	0.67
1	1	1	no	0.26	0.72
1	0	0.25	no	5.3	0.13
0	1	0.25	no	0.034	0.27
1	1	0.25	no	2.0	0.34
1	0	1	yes	0.77	0.31
0	1	1	yes	0.27	0.67
1	1	1	yes	0.34	0.72
1	0	0.25	yes	6.6	0.13
0	1	0.25	yes	0.087	0.28
1	1	0.25	yes	2.5	0.34

(SHL) with $d_h\omega_h = 1$ km s^{-1} on top of the defect layer. This yields a somewhat better matching of the evanescent waves and so improves the bottleneck to the solid.

Besides the resistance ratio W_h/W_s, we show also the average absorption coefficients, W_s/W_0 (see the previous section). Values around 50% are to be expected from experiments. It is obvious from table 1 that large values for W_h/W_s, i.e. strong bottlenecks, can be obtained in some cases, and substantial W_s/W_0 values in other cases. In the last line we have found a trade-off which yields the right order of magnitude for both quantities. But we were not able to find a really convincing set of parameters where both W_h/W_s and W_s/W_0 were large enough to account for the experiments.

10. Conclusions

We investigated the consequences of a model where the Kapitza transport is caused by a thin surface layer whose phonon scattering or absorption properties are phenomenologically described by complex elastic constants and complex mass density. By including the backscattering of phonons we find that the Kapitza resistance can be expressed as a series connection of an inner resistance ascribed to the layer–solid interface and an outer resistance ascribed to the layer–helium interface. Most experimental findings could be explained if the inner resistance were to dominate. Unfortunately, the interaction of the layer via evanescent waves inherent in this model is numerically not quite strong enough to lower the outer resistance sufficiently.

Improvements may be achieved by including the effects of the rotons and of the possible roughness of the layer surface. Furthermore it might be unavoidable to study microscopic possibilities for a direct, non-local interaction of the layer with the helium, e.g. by van der Waals forces.

Acknowledgments

We would like to thank W Dietsche for numerous discussions. One of us (HK)

is grateful to N S Shiren for important suggestions, and to F Scaramuzzi and D Goodstein for discussions and continuous interest.

References

[1] Kapitza P L 1941 *Sov. Phys.–JETP* **11** 1
[2] Khalatnikov I M 1952 *Sov. Phys.–JETP* **22** 687
[3] Challis L J 1974 *J. Phys. C: Solid State Phys.* **7** 481
[4] Guo C J and Maris H J 1972 *Phys. Rev. Lett.* **29** 855
[5] Kinder H and Dietsche W 1974 *Phys. Rev. Lett.* **33** 578
[6] Haug H and Weiss K 1972 *Proc. 4th Int. Cryogenic Engineering Conf.* (Eindhoven: IPC Science & Technology) p 129; 1972 *Phys. Lett.* **40A** 19; 1972 *Proc. Int. Conf. on Phonon Scattering in Solids* (Paris: Service de Documentation du CEN Saclay) ed H J Albany p 386
[7] Peterson R E and Anderson A C 1972 *Phys. Lett.* **40A** 317
[8] Sherlock R A, Mills N G and Wyatt A F G 1975 *J. Phys. C: Solid State Phys.* **8** 300
[9] Challis L J, Dransfeld K and Wilks J 1961 *Proc. R. Soc.* A **260** 31
[10] Goodstein D, Paternò G, Scaramuzzi F and Táborek P 1981 *Nonequilibrium Superconductivity, Phonons, and Kapitza Boundaries (Nato ASI Ser. B 65)* ed K E Gray (New York: Plenum) p 665
[11] Buechner J S and Maris H J 1975 *Phys. Rev. Lett.* **34** 316
[12] Weber J, Sandmann W, Dietsche W and Kinder H 1978 *Phys. Rev. Lett.* **40** 1469
[13] Kinder H, Weber J and Dietsche W 1980 *Phonon Scattering in Condensed Matter* ed H J Maris (New York: Plenum) p 173
[14] Basso H C, Dietsche W, Kinder H and Leiderer P 1984 *Phonon Scattering in Condensed Matter (Ser. Solid State Sci. 51)* ed W Eisenmenger, K Laßmann and S Döttinger (Berlin: Springer) p 212
[15] Basso H C, Dietsche W and Kinder H 1984 *Proc. LT17* ed U Eckern, A Schmid, W Weber and H Wühl (Amsterdam: Elsevier) p 465; 1986 *J. Low Temp. Phys.* **65** 247
[16] Köster L, Wurdack S, Dietsche W and Kinder H 1986 *Phonon Scattering in Condensed Matter V (Ser. Solid State Sci. 68)* ed A C Anderson and J P Wolfe (Berlin: Springer) p 171
Köster L, Colli A, Wurdack S, Dietsche W and Kinder H 1990 *Z. Phys.* B **80** 275
[17] Folinsbee J T and Harrison J P 1978 *J. Low Temp. Phys.* **32** 469
Táborek P and Goodstein D 1979 *J. Phys. C: Solid State Phys.* **12** 4737
[18] Kinder H 1981 *Physica* B **107** 549
[19] Hunklinger S and Raychaudhuri A K 1986 *Prog. Low Temp. Phys.* **9** 265
[20] Kinder H and Weiss K 1986 *Phonon Scattering in Condensed Matter V (Ser. Solid State Sci. 68)* ed A C Anderson and J P Wolfe (Berlin: Springer) p 218
[21] Jäckle J, Piché L, Arnold W and Hunklinger S 1976 *J. Non-Cryst. Solids* **20** 365
[22] Aki K and Richards P G 1980 *Quantitative Seismology* vol I (San Francisco: Freeman)
[23] Weis O 1979 *Z. Phys.* B **34** 55
[24] Wilks J 1967 *The Properties of Liquid and Solid Helium* (Oxford: Clarendon)
[25] McSkimin H J 1953 *J. Appl. Phys.* **42** 988
[26] Hunklinger S and Arnold W 1976 *Physical Acoustics* vol XII ed W P Mason and R N Thurston (New York: Academic) p 155
[27] Stephens R B 1973 *Phys. Rev.* B **8** 2896
[28] Zinov'eva K N 1980 *Sov. Phys.–JETP* **52** 996
Zinov'eva K N and Semenov S 1993 *Phonon Scattering in Condensed Matter VII* ed M Meissner and R O Pohl (Heidelberg: Springer)
[29] Koos G L, Every A G, Northrop G A and Wolfe J P 1983 *Phys. Rev. Lett.* **51** 276
[30] Shiren N S 1981 unpublished calculations
[31] Northrop G A and Wolfe J P 1985 *Nonequilibrium Phonon Dynamics (NATO ASI Ser. B 124)* ed W E Bron (New York: Plenum) p 165
[32] Marx D and Eisenmenger W 1982 *Z. Phys.* B **48** 277
[33] Swanenburg T J B and Wolter J 1973 *Phys. Rev. Lett.* **31** 693
Kinder H, De Ninno A, Goodstein D, Paternò G, Scaramuzzi F and Cunsolo S 1985 *Phys. Rev. Lett.* **55** 2441
[34] Wichert K H, Höß C and Kinder H 1992 *Phonon Scattering in Condensed Matter VII* ed M Meissner and R O Pohl (Heidelberg: Springer)